Eddy correlation measurements of the air/sea flux of dimethylsulfide over the North Pacific Ocean

C. A. Marandino,[1] W. J. De Bruyn,[2] S. D. Miller,[1,3] and E. S. Saltzman[1]

[1] Shipboard measurements of air/sea fluxes and sea surface concentrations of dimethylsulfide (DMS) were made over the tropical and midlatitude North Pacific Ocean. Atmospheric pressure chemical ionization mass spectrometry was used to measure DMS levels in ambient air and in air equilibrated with surface seawater drawn from a depth of 5 m. Air/sea fluxes were obtained using eddy covariance. Corrections and uncertainties involved in the calculation of fluxes from shipboard data are discussed. The surface ocean DMS concentrations measured during this study ranged from 1 to 10 nM, and atmospheric mixing ratios ranged from 20 to 1000 ppt. Air/sea fluxes ranged from 0.47 to 39 μmol m^{-2} d^{-1}. Most of the variance in the fluxes can be accounted for by variations in sea surface concentration (37%) and wind speed (19%). Gas transfer coefficients derived from the measurements are generally consistent with those derived from deliberate inert gas tracer experiments and eddy covariance measurements of CO_2. The gas transfer coefficients exhibit wind speed dependence, but the variance in the data is sufficiently large that they do not constrain the functionality of the wind speed dependence of gas exchange.

Citation: Marandino, C. A., W. J. De Bruyn, S. D. Miller, and E. S. Saltzman (2007), Eddy correlation measurements of the air/sea flux of dimethylsulfide over the North Pacific Ocean, *J. Geophys. Res.*, *112*, D03301, doi:10.1029/2006JD007293.

1. Introduction

[2] Air/sea gas exchange is an important component of the atmospheric budgets of many climate-active trace gases such as CO_2, DMS, and N_2O. The air/sea flux is described by the expression

$$F = k\Delta C = k\left(C_w - \frac{C_a}{H}\right) \qquad (1)$$

where F is the flux, k is the total gas transfer coefficient (or piston velocity), ΔC is the concentration difference between the bulk phases of air (C_a) and water (C_w), and H is the Henry's law solubility constant. The gas transfer coefficient encapsulates both diffusive and turbulent processes at or near the air/sea interface, and represents underlying physical processes that drive gas exchange. Gas exchange is primarily driven by shear generated turbulence in both the atmosphere and ocean. As such, the gas transfer coefficient is often parameterized as a function of wind speed as a surrogate for wind shear/stress. Other factors such as buoyancy-driven motion, microlayer thickness, bubbles, and rain also play a significant role in gas exchange [*Frew*,

1997; *Liss and Merlivat*, 1986; *Ho et al.*, 2004]. The gas transfer coefficient scales with Schmidt number (Sc),

$$k_a = k_b\left(Sc_a\Big/Sc_b\right)^n \qquad (2)$$

where n lies in the range of $-1/2$ to 2/3. Equation (2) illustrates that the gas transfer coefficient for different gases can be compared if the Schmidt number for a given temperature and salinity is known.

[3] Parameterizations for the wind speed dependence of k have been derived from water-side deliberate tracer experiments using inert gases [*Wanninkhof et al.*, 1985; *Nightingale et al.*, 2000; *Watson et al.*, 1991] and from eddy covariance measurements of CO_2 [*McGillis et al.*, 2001]. The oceanic radiocarbon budget [*Broecker et al.*, 1985; *Wanninkhof*, 1992] provides an important constraint on the long-term average gas exchange rate over large spatial scales. Because the chemistry and biology of the air/sea interface are poorly understood, it is not known whether the parameterizations, derived from inert gases, hold for more reactive gases. There is some evidence that the interface itself may be a reactive medium for some biologically active gases [*Conrad and Seiler*, 1988; *Zhou and Mopper*, 1997; *Upstill-Goddard et al.*, 2003].

[4] Micrometeorological flux measurement techniques, such as eddy correlation, gradient flux, and relaxed eddy accumulation, have the potential to measure fluxes of many gases, on smaller temporal/spatial scales than tracer experiments. Because the temporal and spatial scales of these techniques are similar to the scales of variability in many of the physical forcings on gas exchange, these approaches may provide new insight into the factors influencing air/sea

[1]Department of Earth System Science, University of California, Irvine, California, USA.
[2]Department of Physical Sciences, Chapman University, Orange, California, USA.
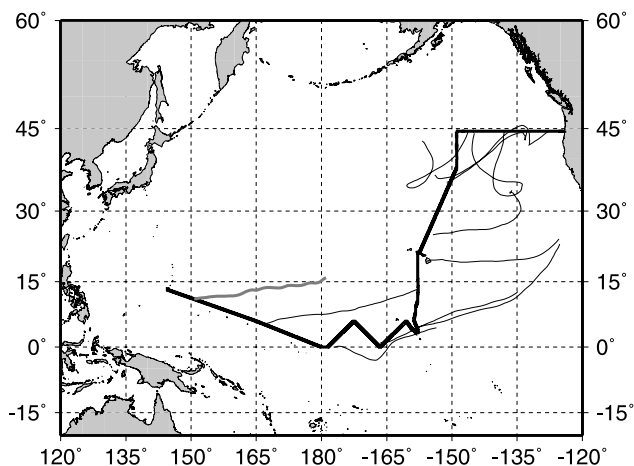[3]Now at Atmospheric Sciences Research Center, Albany, New York, USA.

Figure 1. PHASE I cruise track. Lines originating from the cruise track represent isentropic 5 day back trajectories.

gas exchange. However, there are numerous challenges associated with the implementation of these techniques at sea, including issues involving sensor motion and flow distortion associated with various platforms [*Edson et al.*, 1998]. Recently, considerable progress has been made and eddy correlation has been successfully used to the measure air/sea flux for CO_2 [*Donelan and Drennan*, 1995; *McGillis et al.*, 2001], DMS [*Huebert et al.*, 2004], and acetone [*Marandino et al.*, 2005]. Gradient flux and relaxed eddy accumulation have also been used to determine the air/sea flux and gas transfer coefficients for DMS [*Hintsa et al.*, 2004; *Zemmelink et al.*, 2004].

[5] In this study, we present shipboard measurements in the equatorial and midlatitude North Pacific Ocean from May to July 2004 (Figure 1). The eddy correlation air/sea flux and the air/sea concentration difference of DMS were measured using atmospheric pressure chemical ionization mass spectrometry (API-CIMS). DMS gas transfer coefficients were computed from these data, and the relationship between gas transfer and horizontal wind speed was examined.

2. Methods

2.1. Cruise Description

[6] These measurements were made as part of the Project Halogen Air Sea Exchange (PHASE I) cruise aboard the R/V *Wecoma*. The first leg of the PHASE I cruise started in Guam on 22 May 2004 (DOY 142) and ended in Hawaii on 18 June 2004 (DOY 170). The second leg started in Hawaii on 22 June 2004 (DOY 173) and ended in Newport, Oregon on 3 July 2004 (DOY 184). The cruise track can be separated into four oceanographic regions, starting from DOY 142: warm pool, equatorial upwelling, gyre, and subpolar. Air mass back trajectories show that in the warm pool and equatorial upwelling regions the winds were predominantly easterly and the air was oceanic in origin, while in the gyre and subpolar regions the winds were largely westerly and the air was continentally influenced. Wind speeds were variable and ranged between 0 and 15 m s^{-1} over the entire cruise track. Sea surface temperatures were approximately 30°C in the warm pool and equatorial upwelling regions. The sea surface temperature was 15°–20°C in the gyre region, and 10°–15°C in the subpolar region.

2.2. Eddy Correlation Technique and Experimental Setup

[7] Eddy correlation is a method of directly determining scalar fluxes by computing the covariance between the fluctuations in vertical wind speed and the fluctuations in the scalar quantity [*Lenschow*, 1995]. Three-dimensional winds were measured aboard the R/V *Wecoma* on the forward jackstaff at a height of approximately 10 m above the sea surface, using a Campbell CSAT3 sonic anemometer. Three dimensional platform angular rates and accelerations were measured using a Systron Donner Motion Pak II (MPII) motion sensor. The MPII was mounted rigidly on the same mounting bracket as the anemometer. Speed and course over ground were measured at 1 Hz using a Garmin GPS 16, which was mounted aft on the upper deck. The air sampling intake was located on the jackstaff, approximately 10 m above the sea surface and 60 cm from the anemometer sensing region.

[8] The air intake for DMS analysis consisted of a 5 cm diameter PFA filter housing, with a $^1/_2''$ orifice. The air was pumped through 76 m of $3/8''$ ID Teflon tubing, to the ship's dry lab, where the API-CIMS instrument was located. A schematic of the sampling system is shown in Figure 2. The airflow from the jackstaff inlet was mass flow controlled at 27 L min^{-1} STP to maintain turbulent flow. In the laboratory, a 1.6 L min^{-1} STP airflow was drawn from the main flow through a Nafion membrane dryer (2 feet in length, $^1/_4''$ ID outer tube, 1/16$''$ ID inner tube) into the API-CIMS source. An Aadco clean air generator provided the dry air counterflow for the membrane dryer.

[9] The seawater analyzed in this study was supplied by the ship's continuous flow bow pumping system. The intake for this system was at a depth of 5 m. Approximately 300 cm^3 min^{-1} STP of seawater was directed through a membrane equilibrator, located in the *Wecoma*'s wet lab, approximately 3 m from the API-CIMS instrument. The equilibrator consisted of a 10 cm long 2$''$ ID PFA pipe housing, with a 1 m long, 3 mm ID porous (60–70% porosity) Teflon tube (International Polymer Engineering) as the membrane. An airflow of 25–60 cm^3 min^{-1} STP from the clean air generator was passed through the porous tubing and allowed to equilibrate with the seawater. Complete equilibration was demonstrated by examining the seawater DMS signal as a function of gas flow rate. The equilibrated air stream was then mixed into a 2.5 L min^{-1} STP clean airflow from the Aadco and directed either to waste or to the API-CIMS source. All of the gas flows used in the system were regulated with mass flow controllers, which were calibrated using a Gillian Gilibrator bubble flowmeter. The temperature of the seawater at the equilibrator was continuously logged and exhibited an offset from the sea surface temperature of 0.98°C.

[10] The measurement protocol consisted of alternating seawater and air analyses. The seawater analyses were between 2 and 15 min long and the air measurements were 60 min. The meteorological and motion data were logged as analog signals at 50 Hz, and filtered using a National Instruments SCXI-1143 Butterworth filter with a 15 Hz cutoff frequency. The API-CIMS data were acquired at 10 Hz in single ion monitoring mode. The API-CIMS data system provided a digital output, which was logged by the
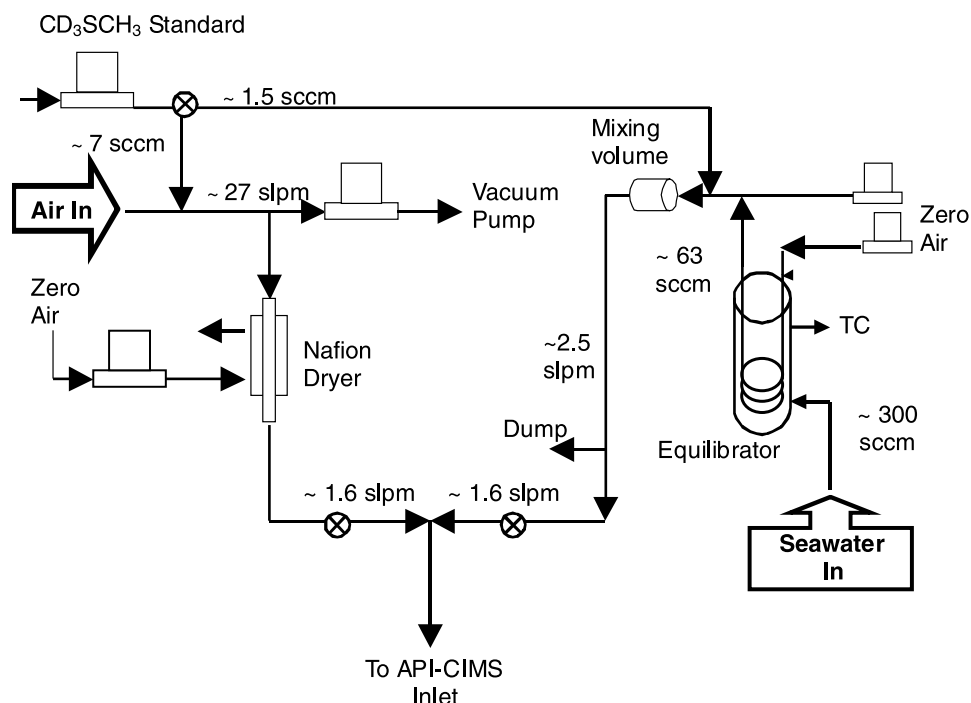
Figure 2. Schematic of API-CIMS experimental setup. On the left is the air sampling side and on the right is the water sampling side. Flow rates are given in standard cubic centimeter per minute and standard liter per minute.

meteorological data acquisition system to provide synchronization between the two data streams.

2.3. API-CIMS Instrument

[11] A schematic of the API-CIMS instrument is shown in Figure 3. The inlet of the API-CIMS instrument used in this study is a glass-lined stainless steel tube containing a cylindrical radioactive ^{63}Ni foil, which is a low-energy beta emitter [*Mitchell*, 2001]. As air passes through the tube, the emitted beta particles initiate a series of ion-molecule reactions resulting in the formation of protonated water and water clusters, where n and m indicated the number of water molecules:

$$H^+(H_2O)_{n-1} + H_2O + N_2 \leftrightarrow H^+(H_2O)_n + N_2 \qquad (3)$$
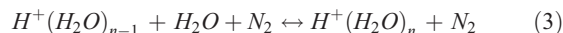
The protonated water clusters can protonate DMS, resulting in the formation of the DMSH$^+$ (H$^+$CH$_3$SCH$_3$) ion detected by the mass spectrometer,

$$H_3O^+(H_2O)_n + CH_3SCH_3 \leftrightarrow H^+(CH_3SCH_3)(H_2O)_m$$
$$+ H_2O_{n+1-m} \qquad (4)$$
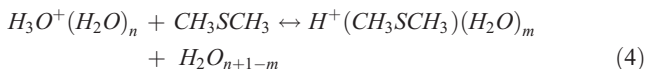
[12] At atmospheric pressure and high humidity, the higher-order water clusters ((H$_2$O)$_{n>1}$) dominate the positive ion spectrum in air. This reduces the sensitivity for DMS analysis because the proton affinity of DMS is lower than that of the higher-order water clusters. In addition, high humidity causes the DMS signal to be spread across many different clusters, lowering the signal of each individual DMS-containing ion [*Sunner et al.*, 1988a, 1988b]. In order to optimize the sensitivity of the instrument for DMS, the API-CIMS inlet is heated to 450°C, and the air stream was dried prior to entering the inlet using a Nafion membrane dryer. Heating and drying drives the water ion distribution

to smaller clusters (n = 1, 2, 3) and favors the formation of DMSH$^+$ [*Sunner et al.*, 1988a, 1988b; *Bandy et al.*, 2002]. Figure 4 shows positive ion spectra of marine air with 75% relative humidity, with and without the Nafion dryer. These spectra illustrate that drying causes a shift toward smaller water clusters, with a decrease in the signal at mass/charge
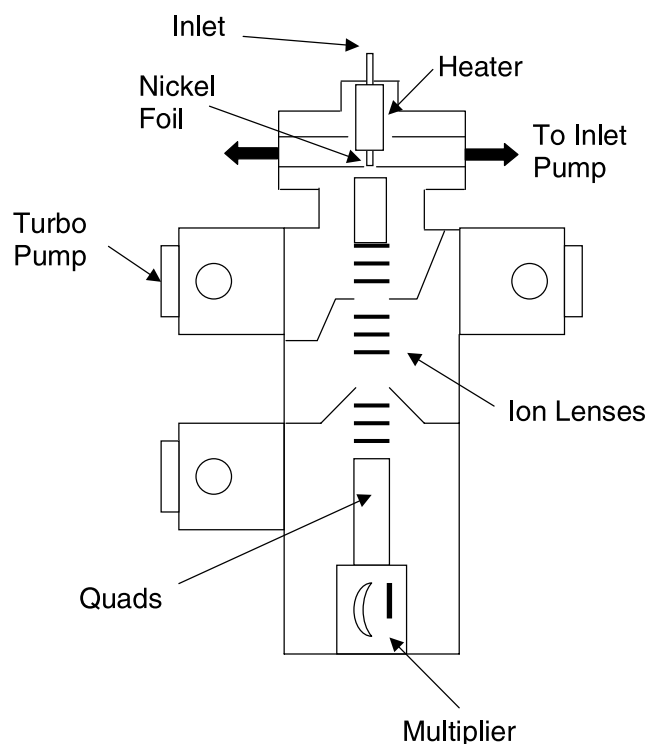

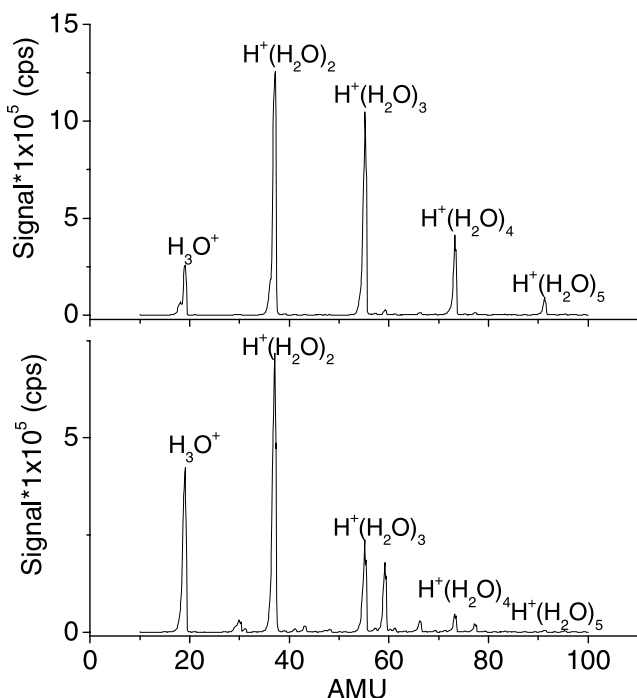
Figure 3. Schematic of API-CIMS.

Figure 4. Positive ion spectrum of marine air just north of Hawaii (21°N; DOY 174). (top) Without Nafion dryer. (bottom) With Nafion dryer. Labeled peaks correspond to $H^+(H_2O)_n$.

(m/z) 37, $H^+(H_2O)_2$, and an increase in the signal at m/z 19, $H^+(H_2O)$. However, it has been demonstrated in the laboratory that when the level of water vapor is too low the sensitivity for DMS decreases because there is not enough water vapor to undergo charge transfer reactions with DMS.

[13] The API-CIMS used in this study was constructed in our laboratory, using a $^3/_4''$ quadrupole mass filter (ABB Extrel Corp.). The design of the high vacuum chamber and ion optics is based on that of *Eisele and Tanner* [1993]. Ions enter the mass spectrometer through a 225 μm diameter pinhole. The vacuum system consists of three differentially turbo-pumped chambers, at pressures of approximately 5×10^{-3} Torr, 4×10^{-4} Torr, and 1×10^{-5} Torr, respectively. The ions are electrostatically steered to the entrance of the mass filter and are detected using an ion multiplier, preamplifier-discriminator, and counter. The instrument is controlled by software running on the National Instruments real-time operating system (NI PXI-8145). The user interface is a PC-based Visual Basic program, which communicates with the real-time computer via TCP-IP.

2.4. Calibration

[14] DMS in air was quantified by isotope dilution using trideuterated DMS (CD_3SCH_3) as the internal standard. This standard was prepared in our laboratory as a 2.15 ± 0.13 ppm mixture in N_2 in a high-pressure aluminum cylinder. The cylinder was calibrated in the laboratory by direct comparison to a Vici-Metronics DMS permeation tube using the API-CIMS instrument. The output of the permeation tube was determined gravimetrically. The isotope-labeled standard tank was calibrated both in the laboratory and in the field. These results are based on the first laboratory com-

parison, before the start of the field campaign. The precision of the field calibration was poor because of instability in the permeation oven temperature under field conditions.

[15] The standard was added to the outside air and equilibrator air streams, to obtain mixing ratios of approximately 670 ppt and 1185 ppt, respectively. The standard was monitored continuously at m/z 66. For air measurements, the internal standard was delivered at 7 cm^3 min^{-1} STP to the air intake on the jackstaff and mixed into the sampled air, so it was subject to transport through the same long run of tubing and Nafion drier as the air sample. For seawater analysis, 1.5 cm^3 min^{-1} STP of standard was mixed into the dilution air at the same point as the return air from the membrane equilibrator.

2.5. DMS Detection and Sensitivity

[16] The DMS signals, both $H^+CH_3SCH_3$ and $H^+CD_3SCH_3$, were acquired in single ion monitoring mode at m/z 63 and 66, respectively. The ambient DMS signal was converted to mixing ratio using the signal from the isotope-labeled internal standard (CD_3SCH_3), after blank removal. Two types of blanks were accounted for: (1) positive interference at m/z 66 in ambient air or air equilibrated with seawater (i.e., unrelated to the standard tank) and (2) the presence of a small fraction of unlabeled DMS (i.e., m/z 63) in the isotope labeled standard. The magnitude of the first blank was determined by sampling ambient air without standard added. The magnitude of the second blank was determined by calculating the difference in m/z 63 between an ambient air analysis with and without the standard added. System blanks were monitored every 12 hours. The instrument sensitivity (cps ppt^{-1}) was determined by dividing the standard count rate (cps) by the mixing ratio of the internal standard, scaled by the ratio of the gas flow rates.

[17] The concentration of DMS in seawater was calculated in the same manner as the air signal. The mixing ratio of DMS was calculated from the standard instrument sensitivity, in the equilibrated air stream. The concentration of DMS in surface seawater was calculated by converting the DMS mixing ratio in the equilibrated air stream to partial pressure, and using the Henry's law constant for seawater in M atm^{-1} [*Dacey et al.*, 1984].

[18] Variations in instrument sensitivity during the cruise are shown in Figure 5. The instrument exhibited slightly more sensitive response during water analyses than during air analyses. This could be due to minor differences in water vapor content in the two sample streams, where the water stream contained less water vapor because it was diluted with dry air. It could also be due to a larger pressure drop for air measurements at the API-CIMS inlet due to the long lengths of tubing used for air side sampling. Instrument sensitivity decreased dramatically late in the cruise. This decrease was associated with a decrease in ambient air temperature and absolute humidity, which occurred as the ship headed northward from the tropics into cooler waters. Additional loss of sensitivity occurred on the last day of sampling because of a blockage of the API-CIMS pinhole.

2.6. Ancillary Data

[19] Oceanographic and meteorological data gathered by the *Wecoma*'s instruments included sea surface temperature,
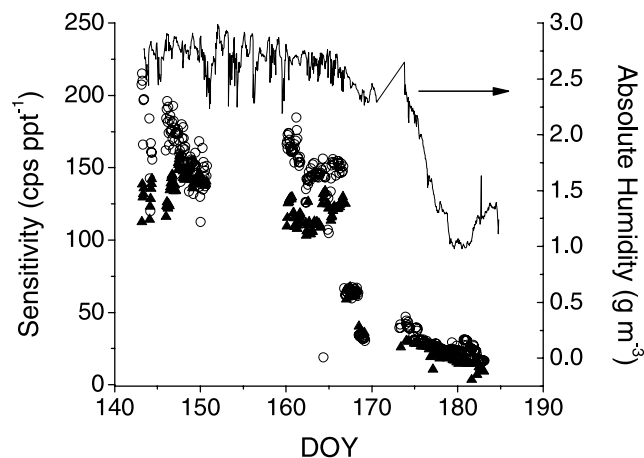
Figure 5. API-CIMS instrument sensitivity for DMS during the PHASE 1 cruise, determined from air (solid triangles) and water (open circles) analyses. Absolute humidity during PHASE 1 is plotted as a solid line (plotted on right axis).

fluorescence, salinity, wind speed and direction, relative humidity, and air temperature. Atmospheric ozone and NO_x were monitored continuously using a Thermo Model 42C and 49C, respectively. Atmospheric and surface seawater concentrations, and depth profile measurements of several anthropogenic and biogenic gases (e.g., CH_3Cl, CH_3Br, PCE) were also made. Reported chlorophyll concentrations are monthly averaged June, 2004 MODIS data (0.09° × 0.09°). The chlorophyll value for each hourly cruise track latitude and longitude was obtained by averaging 4–8 nearest neighbors.

3. Eddy Covariance Data Processing and Error Analysis

3.1. Density Correction

[20] As discussed by *Webb et al.* [1980] fluctuations in air density caused by variations in temperature and water vapor can result in fluctuations in concentration of trace gases. As a consequence, surface fluxes in heat and water vapor give rise to spurious trace gas fluxes by eddy covariance. In this study, temperature fluctuations were damped by heat transfer in the long tubing lines. Likewise, water vapor fluctuations were damped by the Nafion membrane (data not shown). The damping of these fluctuations minimized the need for a density correction. The magnitude of density-induced apparent DMS flux was estimated by computing the covariance between the isotope labeled DMS standard and vertical wind speed. The isotope is delivered to the air inlet at a constant flow rate, and should exhibit concentration fluctuations reflecting only the variations in air density. These apparent fluxes were less than 4% of the measured ambient DMS fluxes, after normalizing for the difference in concentration between the isotope and ambient DMS.

3.2. Tubing Delay

[21] The time required to pump air down the inlet tubing resulted in a time delay between the sonic anemometer and DMS signals. The delay in the tubing was determined

experimentally to be approximately 12 s by using a solenoid valve to inject a pulse of isotope labeled DMS into the inlet, and observing its arrival time at the API-CIMS instrument. Laboratory experiments in which the isotope labeled standard was injected into various lengths of tubing indicate that no chemical loss occurs in the tubing. For each 1-hour flux calculation, we found the maximum covariance by shifting the vertical wind and DMS signals within a centered 4 s window about the nominal 12 s lag (i.e., in the range of 10–14 s). The lag times obtained in this way had a standard deviation of approximately 5%, which is within the variability expected because of the physical separation of the anemometer sensing volume and the air inlet and variations in apparent wind speed and direction.

3.3. Motion Correction

[22] Measured winds on a moving ship are contaminated by platform motion. The sonic anemometer wind data were corrected following *Edson et al.* [1998], and the corrected winds were "rotated" such that the mean vertical wind velocity was equal to zero [*McMillen*, 1988]. Figure 6 shows an example of a vertical wind power spectrum and a cospectrum of vertical wind and DMS with and without motion correction. In the uncorrected power spectrum, the
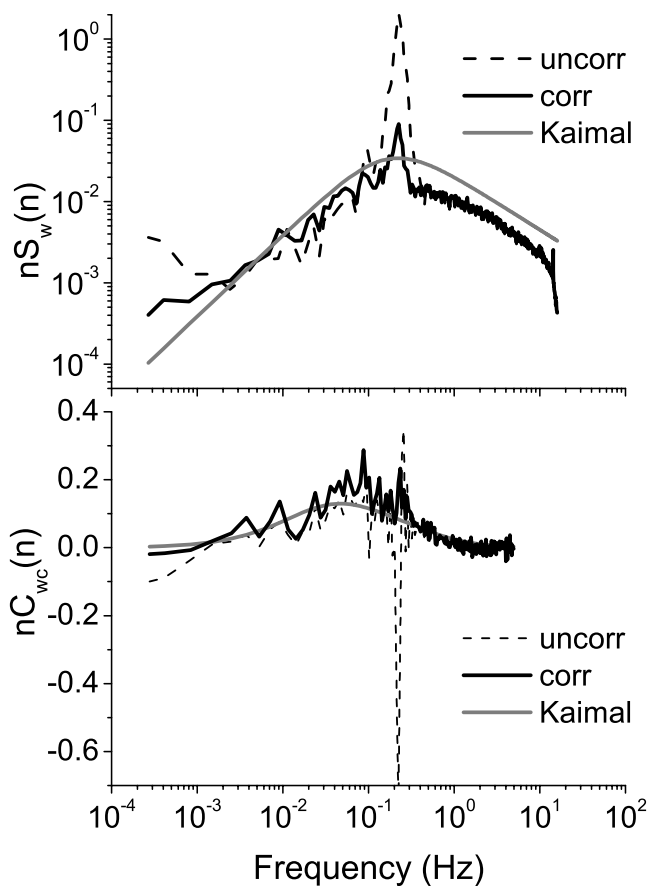

Figure 6. Effects of motion correction on (top) vertical wind power spectrum (50 Hz sampling frequency) and (bottom) DMS cospectrum (10 Hz sampling frequency). Dashed and solid lines are the uncorrected and corrected spectra. Shaded lines are computed spectra after *Kaimal et al.* [1972]. Data are from DOY 147, 8°N.

Table 1. Eddy Covariance Data Corrections and Associated Uncertainties

Correction	Estimated Uncertainty, %
Motion/flow distortion	±20
Low frequency	±10
High frequency	±10
Combined uncertainty	±25

dominant frequency is 0.2 Hz (5 s), corresponding to the period of ocean swell. In the corrected power spectrum, the power at 0.2 Hz is reduced by about 20 fold. The shapes of the corrected vertical wind spectrum and vertical wind and DMS cospectrum are similar to that of the *Kaimal et al.* [1972] curves for each component. The motion corrected output for the horizontal components of wind were further corrected for the translational motion of the ship. The gps measurement of the ship's speed over ground in m s^{-1} was subtracted from the x (U) component of the corrected wind before the mean horizontal wind speed was computed. For the majority of the cruise the ship traveled at an average of 4 m s^{-1}. The uncertainty in the flux due to motion correction is estimated to be 20% [*Edson et al.*, 1998] (Table 1).

3.4. Flow Distortion

[23] Flow distortion caused by the bow of the ship can contaminate flux measurements, and is difficult to quantify. Generally, scalar fluxes are less affected by flow distortion than vector quantities like momentum [*Pedreros et al.*, 2003]. A detailed study of the flow distortion around the *Wecoma* is beyond the scope of this work. Instead, we restricted the data used in the calculation of gas exchange coefficients to those with relative wind directions within ±60° from the front of the ship.

3.5. Frequency Corrections

[24] Large eddies contributing to turbulent fluctuations in the atmosphere may be insufficiently sampled in 1 hour flux records, but may contribute a significant portion of the flux [*Sakai et al.*, 2001]. In some of the records from this study, large features are present in cospectra between 1×10^{-4} and 5×10^{-3} Hz. These apparent fluxes are both positive and negative in sign, while the higher-frequency regions of the cospectra are always positive. We conclude that these low-frequency features do not represent air/sea flux, but are artifacts of undersampling large eddies. Therefore a record was excluded from analysis if either the temperature or the DMS flux at 5×10^{-3} Hz deviated from the full flux by more than 30%. Fifty-one records were excluded from analysis (23%). Visual inspection of the time series showed that these records exhibited signs of changing conditions during each run. The uncertainty in the measurement of the low-frequency portion of the flux records was estimated to be 10%, which was the average amount of the total flux at frequencies lower than 5×10^{-3} Hz (Table 1).

[25] Because a long length of tubing was used to sample the air from the bow, corrections are made for the loss of high-frequency fluctuations in the tubing [*Lenschow and Raupach*, 1991; *Massman*, 1991]. An empirical correction method was used, based on the observed loss of frequency content in the DMS signal relative to that of the sonic temperature signal, which is an open path measurement made directly on the mast. We assume that the temperature and DMS frequency distributions in the atmosphere are similar because both are scalar surface fluxes. Simultaneous temperature and DMS signals are shown in Figure 7, as the cumulative sums of their respective cospectra, summing from low to high frequency. To make a direct comparison between the frequency content of the signals, the cumulative sums are normalized by their respective total fluxes. Compared to the wT cumulative sum, the wDMS cumulative sum appears attenuated at frequencies greater than 0.4 Hz. The correction was made by determining the frequency corresponding to 50% of the cumulative temperature flux, f_{50}. It was assumed that DMS should have the same f_{50}, so the DMS flux at this frequency was multiplied by a factor of
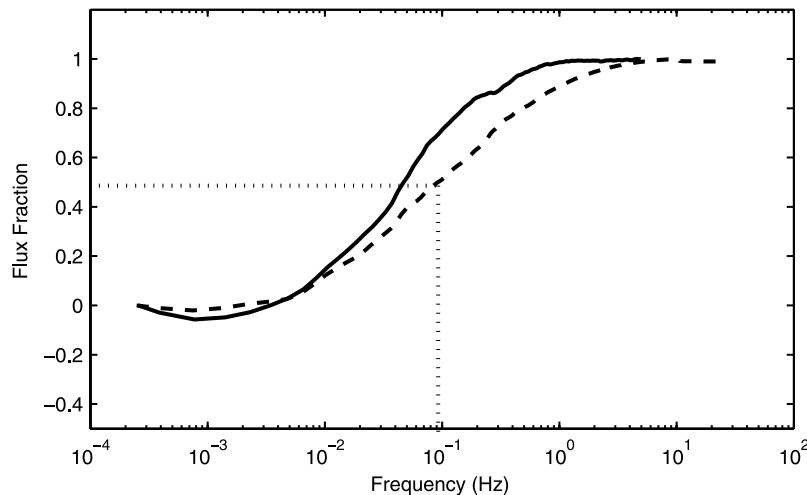

Figure 7. Low-to-high-frequency cumulative sums of DMS and vertical wind (solid line) and temperature and vertical wind (dashed line) cospectra from (28°N, DOY 174). Both cumulative sums are normalized by their respective fluxes (flux fraction of 1). The right angle dotted lines indicate f_{50} for the temperature cumulative sum, which is used to determine where f_{50} for the DMS flux would be if not for high-frequency attenuation in the tubing.
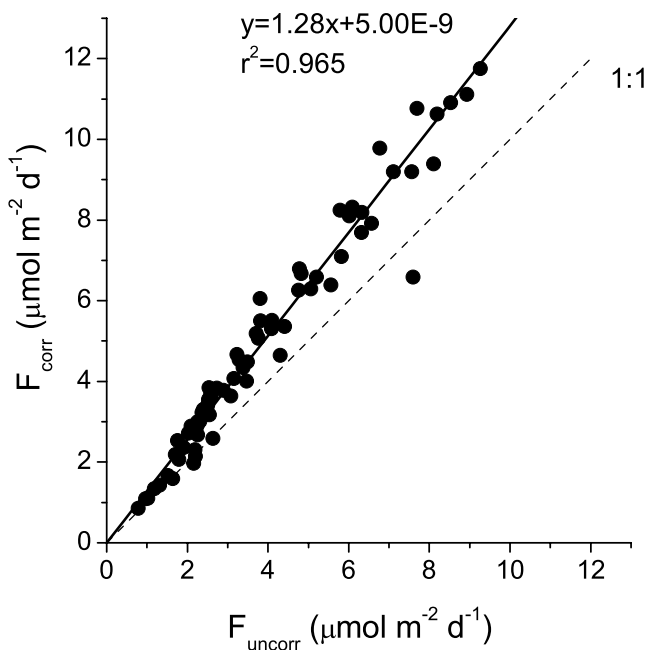
Figure 8. Comparison of high-frequency-corrected flux to uncorrected flux for data used to compute k (Table 2).

two. This correction assumes that no frequency content was lost in the DMS signal at or below f_{50}. This is likely, because similar results were obtained while making the correction using f_{40}, f_{50}, f_{60}, and f_{75}. Assuming that there is no attenuation of the DMS fluctuations in the tubing at f_{40}, the sensitivity of the correction made at each value of F can be determined by computing the ratio of the fluxes corrected at each F to the corrected flux at f_{40}. The computed ratios were 0.92, 0.84, and 0.75 for f_{50}, f_{60}, and f_{75}, respectively, indicating that there are significant tubing effects at frequencies as low as f_{60}. The high-frequency correction increases the fluxes, with a mean correction of 28% (Figure 8). The uncertainty associated with the high-frequency correction was estimated to be 10%, which is the sensitivity of the correction made at f_{50}.

3.6. Quality Control

[26] The data were separated into quality control subsets, according to relative wind direction, and the consistency of DMS seawater analyses before and after each flux run. For each 1 hour flux run, the mean relative wind direction was used as an indicator of the likelihood of flow distortion induced by the ship. Measurements of DMS levels in the sea surface were made before and after each flux run, which

separated them by 1 hour. The concentration difference may not have been well represented because of spatial heterogeneity in DMS water concentrations. For each flux record the difference between before and after water levels was divided by the mean of the two records ($\Delta C/C_{avg}$). The best subset of data was further subdivided by using the ratio of the flux at 5×10^{-3} Hz and the full flux, as discussed in section 3.4. This quality control was included as a measure of low-frequency features that may not be due to air/sea exchange and that may increase the scatter in the computed values of the gas exchange coefficient. Table 2 lists the quality control category, criteria, and symbol for each used in Figures 9 and 13.

4. Results and Discussion

4.1. DMS Bulk Water and Air Measurements

[27] The data can be separated into four oceanographic regions: warm pool, equatorial upwelling, gyre, and subpolar (Figure 9). Mean seawater DMS concentrations (Table 3) were highest in the subpolar region, followed by the equatorial upwelling region and the western Pacific warm pool region. DMS seawater concentrations were lowest in the gyre region. The same general trend exists in the mean chlorophyll concentrations. The chlorophyll concentrations were most correlated with seawater DMS concentrations at the subpolar front, which correspond to DOY 178 and 182 in Figure 9. Enhanced seawater DMS concentrations at ocean fronts have been previously reported [Matrai et al., 1996]. The measured DMS levels are in agreement with previous studies [Bates et al., 1993, 1994; Watanabe et al., 1995; Bates and Quinn, 1997; Huebert et al., 2004].

[28] The highest and lowest mean DMS air mixing ratios and flux followed those of the mean seawater DMS concentrations (Table 3). It appears that the variations in the levels of DMS in these regions were due primarily to variations in the air/sea flux rather than in atmospheric mixing or oxidation rate. DMS mixing ratios are in agreement with previously reported values [Andreae et al., 1985, 1988; Bates et al., 1990, 1992; Quinn et al., 1990; Bandy et al., 1992; Berresheim et al., 1995].

4.2. DMS Flux Measurements

[29] DMS air/sea fluxes were uniformly out of the ocean over the entire cruise track, in agreement with the computed concentration differences. Most of the observed variance in the DMS flux can be explained by DMS ocean concentration (37%) and wind speed (19%) (Table 3 and Figures 9 and 10). Given the analytical uncertainties associated with the flux measurements, these two factors are sufficient to explain all the observed variance in the flux. One notable exception to the correlation between DMS flux and seawater

Table 2. Quality Control Criteria for All Measured Fluxes With Symbols Used in Figures 9 and 13

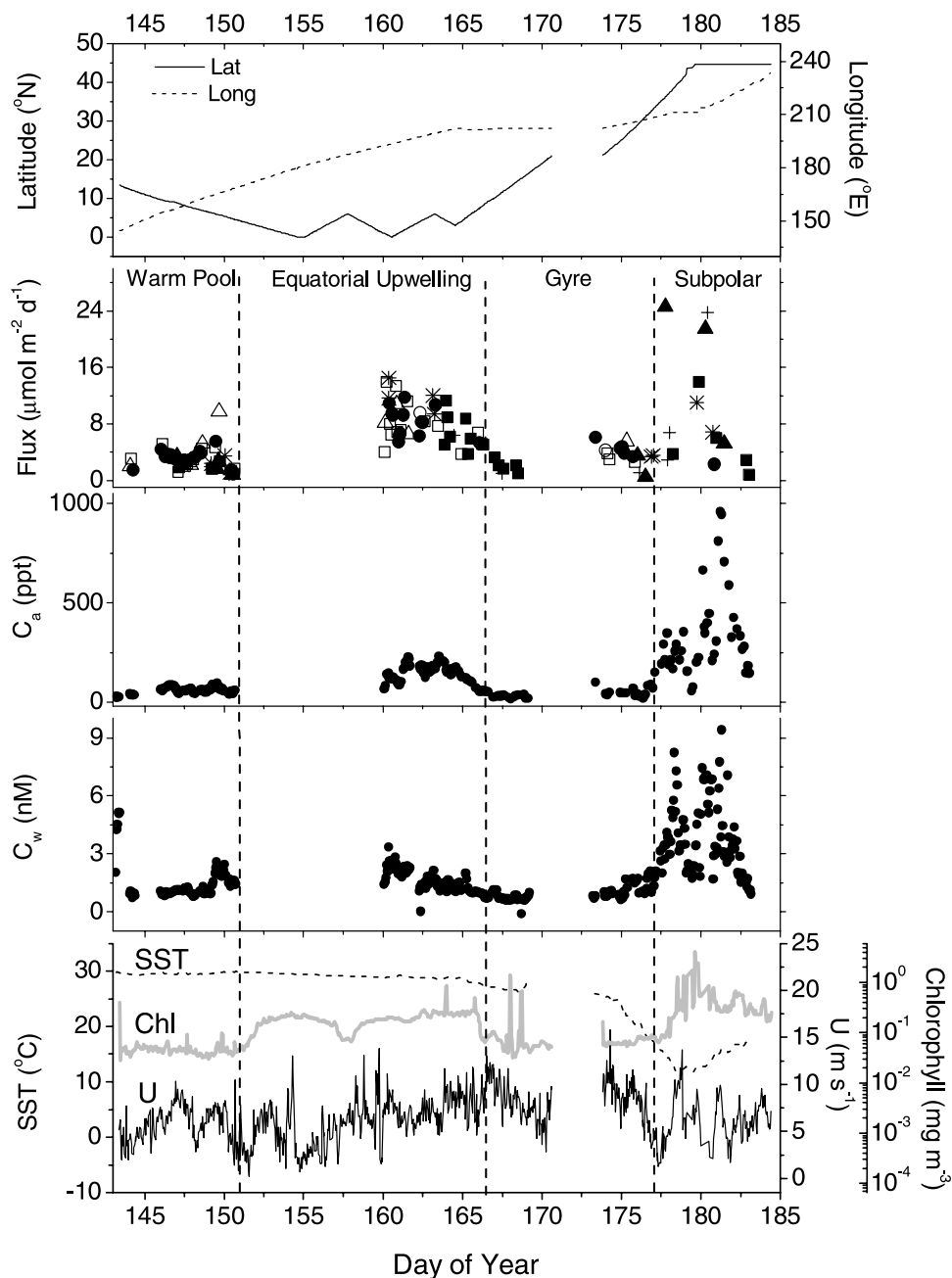| Category	Relative Wind Direction	Seawater DMS$_{SW}$, $\Delta C/C_{avg}$	Low Frequency Features	Symbol
A (used to compute k)	$\leq\pm60°$	≤0.2	<10%	solid circle
B (used to compute k)	$\leq\pm60°$	≤0.2	<20%	open square
C (used to compute k)	$\leq\pm60°$	≤0.2	<30%	open triangle
D	$\leq\pm60°$	n/a (1 measurement)	<30%	open circle
E	$\leq\pm60°$	>0.7	<30%	asterisk
F	$\pm60°$ to $\pm90°$	all	<30%	solid square
G	$\pm90°$ to $\pm120°$	all	<30%	plus
H	$>\pm120°$	all	<30%	solid triangle

Figure 9. DMS measurements during the PHASE I North Pacific cruise (breaks in data due to sampling other compounds and port stop, respectively). Vertical dashed lines indicate oceanographic regions. From top: Cruise track latitude and longitude; eddy correlation air/sea flux measurements by quality control category (see Table 2), where solid circles indicate category A, open squares indicate category B, open triangles indicate category C, open circles indicate category D, asterisks indicate category E, solid squares indicate category F, pluses indicate category G, and solid triangles indicate category H; DMS mixing ratio in air; seawater DMS concentration at 5 m depth; and sea surface temperature, mean horizontal wind speed, and chlorophyll concentration derived from MODIS June 2004 monthly image.

concentration occurred between DOY 177–180 in the subpolar front region. At that time, the ocean concentration of DMS increased several fold, to approximately 8 nM, with only a small increase in flux. DMS levels in air were also low during this period, suggesting that these low fluxes were real. The apparent suppression of the air/sea DMS flux in this region could reflect microlayer effects or strong

subsurface gradients in DMS related to high biological productivity, but there is no direct evidence in support of either explanation.

[30] *Kettle and Andreae* [2000] estimated global DMS air/sea fluxes using climatological winds, sea surface DMS concentrations, and both the *Liss and Merlivat* [1986] and *Wanninkhof* [1992] gas exchange parameterizations. The

Table 3. Mean DMS Levels for Each Oceanographic Region Sampled During PHASE I[a]

Region	DMS_{sw}, nM	DMS_{atm}, ppt	Air/Sea Flux, $\mu mol\ m^{-2}\ d^{-1}$
Warm pool	1.40 ± 0.94	59.3 ± 16.8	2.9 ± 1.5
Equatorial upwelling	1.58 ± 0.60	136.9 ± 49.4	8.2 ± 2.8
Gyre	0.95 ± 0.40	44.3 ± 27.7	3.0 ± 1.6
Subpolar	3.75 ± 1.92	368.1 ± 290.0	10.9 ± 10.9

[a]Uncertainties are 1σ.

DMS fluxes measured during the PHASE 1 cruise fall within the ranges of their calculated fluxes for these regions and seasons.

4.3. Comparison of Eddy Correlation Fluxes With Nocturnal Accumulation of DMS

[31] The diurnal cycle of DMS in marine air is typically characterized by a maximum in the early morning and a minimum during the late afternoon [*Yvon and Saltzman*,
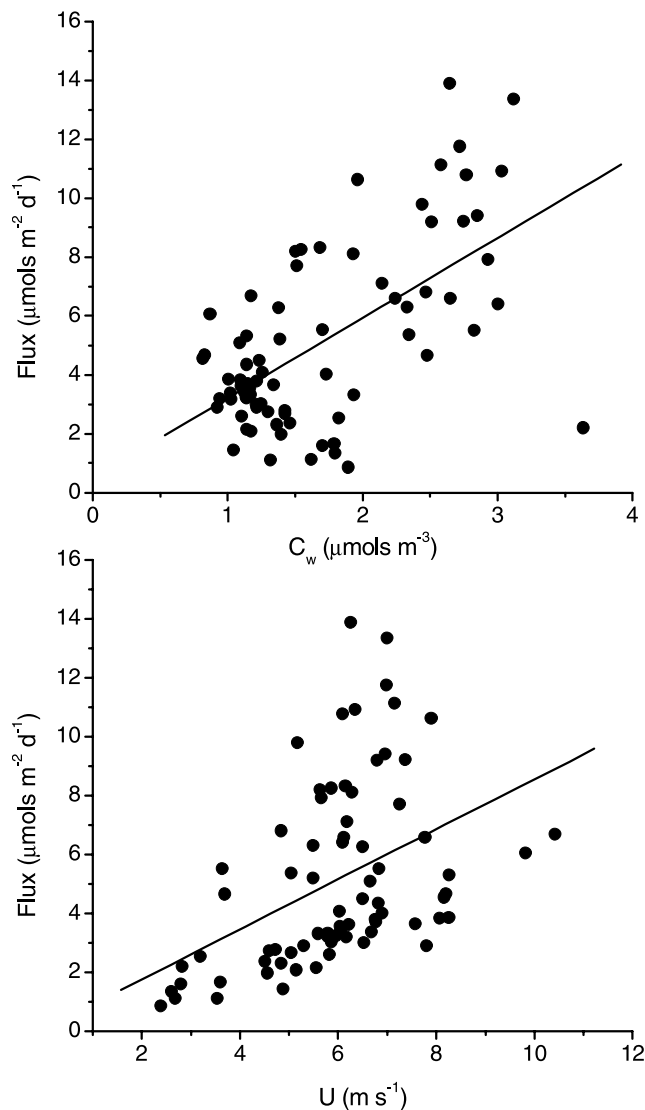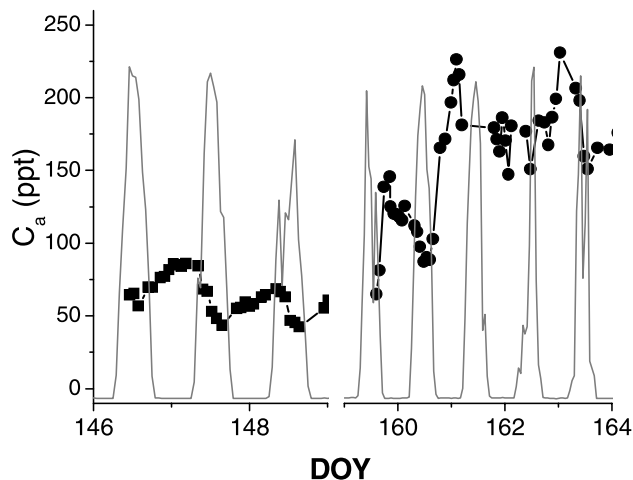

Figure 11. Atmospheric mixing ratios of DMS (solid squares and circles) shown with measured solar irradiation (shaded line) used to calculate air/sea flux of DMS from the nighttime buildup of DMS.

1996; *Bandy et al.*, 1996]. This pattern reflects the dominance of daytime photochemical losses for DMS, and the apparent lack of nighttime reactivity in low NO_x oceanic environments. A diurnal cycle was clearly visible in all oceanographic regions, with the highest DMS levels at approximately 0600 local time (LT) and the lowest at approximately 1700 LT (Figure 11). The nighttime build up of DMS in the atmosphere can be used to calculate the flux of DMS to compare against the measured flux.

[32] For each diel cycle in Figure 11 an air/sea flux was calculated from the slope of the nighttime increase in DMS, assuming a boundary layer height of 1000 m and that no DMS is lost in the boundary layer at night (Figure 12). Horizontal homogeneity was assumed, and the flux is assumed to be zero at the top of the boundary layer, such that

$$\frac{\partial DMS}{\partial t} = -\frac{\partial F}{\partial z} \cong \frac{F_{surface}}{h} \qquad (5)$$

where h represents the height of the boundary layer. The measured eddy covariance fluxes for these periods were averaged and compared against $h * \frac{\partial DMS}{\partial t}$. This is a relatively crude comparison, given the short nature of the data records, and the lack of information about boundary layer structure and mixing. Given this uncertainty, there is reasonable agreement between the two sets of fluxes, as shown in Figure 12.

[33] There are some consistent differences between the shapes of the diel profiles in the different regions. The gyre and warm pool (DOY 146–147, 167–168) exhibited smooth DMS diel cycles that increased steadily through the night and gradually decreased during the day. DMS in the equatorial upwelling region (DOY 160–163), increased steeply at the start of the evening with a sharp decrease just before midnight, perhaps suggestive of DMS oxidation by the nitrate radical.

4.4. Gas Transfer Coefficient Calculations

[34] Gas transfer coefficients were calculated from the highest-quality eddy covariance and seawater DMS measure-

Figure 10. (top) Measured DMS flux versus seawater concentration ($r^2 = 0.37$). (bottom) Measured DMS flux versus mean horizontal wind speed ($r^2 = 0.19$). Both plots show data used to compute k (Table 2).
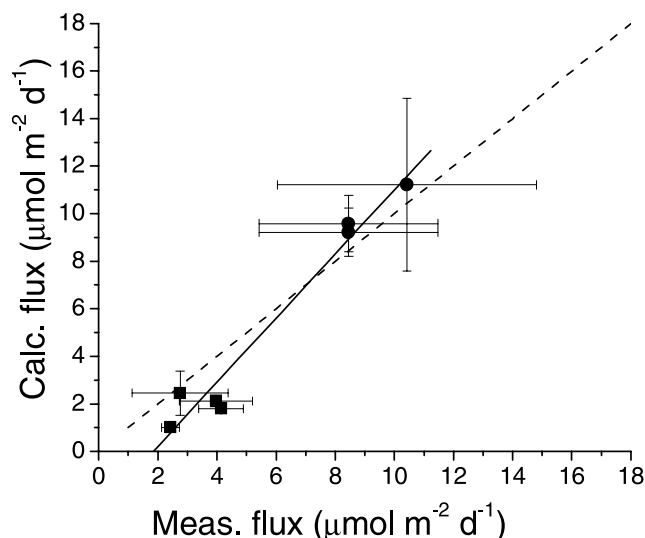
Figure 12. Measured DMS fluxes versus DMS fluxes calculated from nighttime buildup of DMS (solid squares and circles). Symbols correspond to the DOY symbols in Figure 11. The solid line is a linear fit to the data, with a slope of 1.345 (r^2 = 0.96). Error bars are standard deviation (1σ) of the measured fluxes and the slope of the nighttime increase in DMS, respectively.

ments (category A, Table 2), using the expression $k_{DMS} = F/\Delta C$. Gas transfer coefficients were also calculated for the same conditions using the wind speed-dependent parameterizations of *McGillis et al.* [2001], *Wanninkhof* [1992], *Nightingale et al.* [2000], and *Liss and Merlivat* [1986]. All gas transfer coefficients were normalized to a Schmidt number of 720, for DMS in seawater at 25°C [*Saltzman et al.*, 1993], assuming a square root dependence of k on Sc. When comparing field data with the wind speed-based parameterizations it is necessary to distinguish between k_w and k_{total} (i.e., $k_a + k_w$). These parameterizations yield k_w, while the gas transfer coefficients computed from the field measurements (k_{DMS}) are k_{total}. At low temperature and high wind speed, air side resistance can contribute up to 20% of the total resistance to gas exchange for DMS [*McGillis et al.*, 2000]. This is not the case for gas exchange of CO_2, or the inert gas tracers, which are water side controlled. A k_w *for DMS* can be estimated from the PHASE I fluxes, by assuming a wind speed based parameterization for air side gas transfer [*Kondo*, 1975]. For the conditions of PHASE I, this is a small correction that does not significantly affect the k_{DMS} versus wind speed relationship. These gas transfer coefficients are plotted against horizontal wind speed in Figure 13.

[35] Gas transfer coefficients from this study range between 0.4 and 7.6 m d^{-1} over the wind speed range of 2.4–10.4 m s^{-1}. The overall uncertainty in the k values is ±25%. There is a clear wind speed dependence in the data (Figure 13, bottom). Unfortunately, the range of wind speeds for the high-quality data set is limited because higher winds occurred largely in the westerlies, when the winds were following the ship.

[36] At the lower wind speeds encountered in this study, the measured gas exchange coefficients are similar to those obtained from *Wanninkhof* [1992], *Nightingale et al.*

[2000], and *McGillis et al.* [2001], and well above those of *Liss and Merlivat* [1986]. At wind speeds above 5 m s^{-1}, however, these data lie close to the *Liss and Merlivat* [1986] expression, and exhibit a similar wind speed dependence. A similar result was found by *Huebert et al.* [2004], in their shipboard study of eddy covariance DMS fluxes in the Pacific Ocean. Given the uncertainties and scatter in the data, the PHASE I data do not themselves constrain the functionality of the wind speed dependence of k.

[37] The scatter in the PHASE I k versus wind speed relationship should reflect the combined uncertainty in the eddy covariance flux measurements, the variability in the seawater DMS measurements, and the influence on sea surface turbulence of physical processes other than wind speed. The estimated uncertainty of 25% in the individual flux measurements (Table 1), can account for the observed scatter in the data about the previously published parameterizations.

5. Conclusion

[38] This study, like the recent work of *Huebert et al.* [2004], demonstrates the feasibility of making direct, eddy
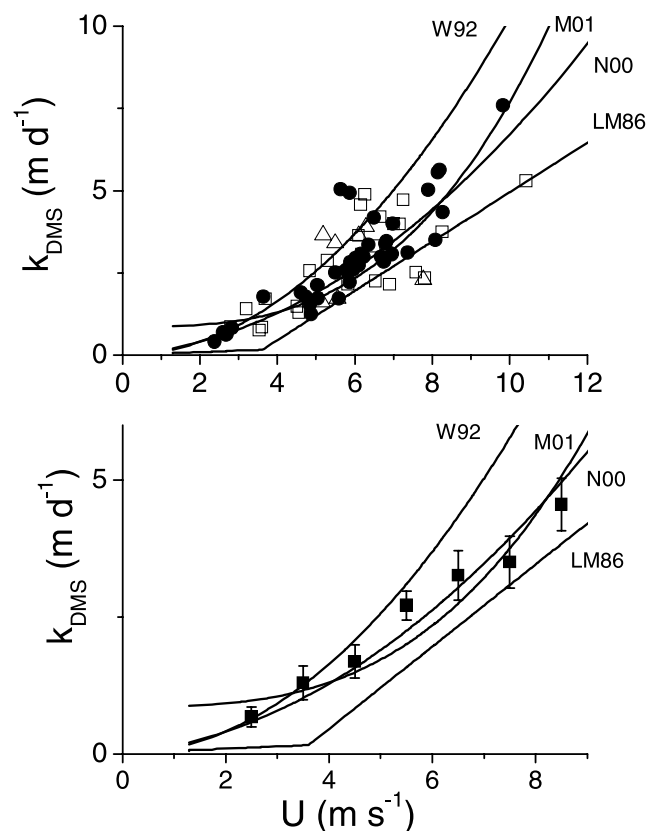

Figure 13. Gas transfer coefficient for DMS (k_{DMS}) versus horizontal wind speed. (top) PHASE I k values separated by the low-frequency quality control criterion (solid circles, open squares, and open triangles). (bottom) Computed k values binned by wind speed in 1 ms^{-1} bins (solid squares). Error bars represent ±1σ. Solid lines are the following parameterizations: M01, *McGillis et al.* [2001]; W92, *Wanninkhof* [1992]; N00, *Nightingale et al.* [2000]; and LM86, *Liss and Merlivat* [1986]. All k_{DMS} values are normalized to Sc = 720.

correlation flux measurements of DMS at sea using chemical ionization mass spectrometry. In this deployment, the measurement frequency was limited by the long length of inlet tubing, but this is a limitation of a specific platform, rather than an inherent limitation of the technique. The relationship between PHASE I computed gas exchange coefficients and wind speed was in general agreement with the k values based on inert tracers (He, SF_6) and CO_2, suggesting that the air/sea exchange of DMS is generally influenced by the same physical forcing mechanisms. It also suggests that the air/sea interface itself is not strongly reactive toward DMS on the timescales of near surface mixing and gas exchange. This field data does not strongly constrain the functionality of the dependence of k on wind speed. The scatter in the k versus wind speed relationship can likely be explained by the uncertainty in the flux measurements, near surface gradients in DMS concentration, and the effect of other physical processes that were not quantified in this study such as buoyancy or current-driven ocean turbulence. A larger database of measurements over a wider range of conditions is needed, with direct measurements of ocean-side turbulence.

[39] Direct measurement of trace gas fluxes, in conjunction with measurements of other physical forcing and near surface turbulence, has the potential to improve our understanding of short-term influences on air/sea flux caused by such processes as rain events, ocean currents, or the presence of organic oceanic surface microlayers. Significantly larger data sets of direct flux measurements are needed, covering the full range of oceanic wind speeds, and both coastal and open ocean environments [*Donelan and Drennan*, 1995; *McGillis et al.*, 2001]. Eddy correlation measurements using API-CIMS also have the potential to directly measure the gas exchange of more reactive trace gases that interact chemically at the air/sea interface.

References

Andreae, M. O., et al. (1985), Dimethylsulfide in the marine atmosphere, *J. Geophys. Res.*, *90*, 12,891.
Andreae, M. O., H. Berresheim, T. W. Andreae, M. A. Kritz, T. S. Bates, and J. T. Merrill (1988), Vertical distribution of dimethyl sulfide, sulfur dioxide, aerosol ions, and radon over the northeast Pacific Ocean, *J. Atmos. Chem.*, *6*, 149.
Bandy, A. R., D. L. Scott, B. W. Blomquist, S. M. Chen, and D. C. Thornton (1992), Low yields of SO_2 from dimethyl sulfide oxidation in the marine boundary layer, *Geophys. Res. Lett.*, *19*, 1125.
Bandy, A. R., D. C. Thornton, B. W. Blomquist, S. Chen, T. P. Wade, J. C. Ianni, G. M. Mitchell, and W. Nadler (1996), Chemistry of dimethyl sulfide in the equatorial Pacific atmosphere, *Geophys. Res. Lett.*, *23*, 741.
Bandy, A. R., D. C. Thornton, F. H. Tu, B. W. Blomquist, W. Nadler, G. M. Mitchell, and D. H. Lenschow (2002), Determination of the vertical flux of dimethyl sulfide by eddy correlation and atmospheric pressure ionization mass spectrometry (APIMS), *J. Geophys. Res.*, *107*(D24), 4743, doi:10.1029/2002JD002472.
Bates, T. S., and P. K. Quinn (1997), Dimethyl sulfide (DMS) in the equatorial Pacific Ocean (1982 to 1996): Evidence of a climate feedback, *Geophys. Res. Lett.*, *24*, 861.

Bates, T. S., J. E. Johnson, P. K. Quinn, P. D. Goldan, W. C. Kuster, D. C. Covert, and C. J. Hahn (1990), The biogeochemical sulfur cycle in the marine boundary layer over the northeast Pacific Ocean, *J. Atmos. Chem.*, *10*, 59.
Bates, T. S., B. K. Lamb, A. Guenther, J. Dignon, and R. E. Stoiber (1992), Sulfur emissions to the atmosphere from natural sources, *J. Atmos. Chem.*, *14*, 315.
Bates, T. S., J. C. Kelly, and J. E. Johnson (1993), Concentrations and fluxes of dissolved biogenic gases (DMS, CH_4, CO, CO_2) in the equatorial Pacific during the SAGA 3 experiment, *J. Geophys. Res.*, *98*, 16,969.
Bates, T. S., R. P. Kicnc, G. V. Wolfe, P. A. Matrai, F. P. Chavez, K. R. Buck, B. W. Blomquist, and R. L. Cuhel (1994), The cycling of sulfur in surface seawater of the northeast Pacific, *J. Geophys. Res.*, *99*, 7835.
Berresheim, H., P. H. Wine, and D. D. Davis (1995), Sulfur in the atmosphere, in *Composition, Chemistry, and Climate of the Atmosphere*, edited by H. B. Singh, p. 253, John Wiley, Hoboken, N. J.
Broecker, W. S., T.-H. Peng, G. Ostlund, and M. Stuiver (1985), The distribution of bomb radiocarbon in the ocean, *J. Geophys. Res.*, *90*, 6953.
Conrad, R., and W. Seiler (1988), Influence of the surface microlayer on the flux of nonconservative trace gases (CO, H_2, CH_4, N_2O) across the ocean-atmosphere interface, *J. Atmos. Chem.*, *6*, 83.
Dacey, J. W. H., S. G. Wakeham, and B. L. Howes (1984), Henry's law constants for dimethyl sulfide in freshwater and seawater, *Geophys. Res. Lett.*, *11*, 991.
Donelan, M. A., and W. M. Drennan (1995), Direct field measurements of the flux of carbon dioxide, in *Air-Water Gas Transfer*, edited by B. Jahne and E. C. Monahan, pp. 677, Aeon Verlag & Studio, Hanau.
Edson, J. B., A. A. Hinton, K. E. Prada, J. E. Hare, and C. W. Fairall (1998), Direct covariance flux estimates from mobile platforms at sea, *J. Atmos. Oceanic Technol.*, *15*, 547.
Eisele, F. L., and D. J. Tanner (1993), Measurement of the gas phase concentration of H_2SO_4 and methane sulfonic acid and estimates of the H_2SO_4 production and loss in the atmosphere, *J. Geophys. Res.*, *98*, 9001.
Frew, N. M. (1997), The role of organic films in air-sea gas exchange, in *The Sea Surface and Global Change*, edited by P. S. Liss and R. A. Duce, pp. 121, Cambridge Univ. Press, New York.
Hintsa, E. J., J. W. H. Dacey, W. R. McGillis, J. B. Edson, C. J. Zappa, and H. J. Zemmelink (2004), Sea-to-air fluxes from measurements of the atmospheric gradient of dimethylsulfide and comparison with simultaneous relaxed eddy accumulation measurements, *J. Geophys. Res.*, *109*, C01026, doi:10.1029/2002JC001617.
Ho, D. T., W. E. Asher, L. F. Bliven, P. Schlosser, and E. L. Gordan (2004), Influence of rain on air-sea gas exchange: Lessons from a model ocean, *J. Geophys. Res.*, *109*, C08S18, doi:10.1029/2003JC001806.
Huebert, B. J., B. W. Blomquist, J. E. Hare, C. W. Fairall, J. E. Johnson, and T. S. Bates (2004), Measurement of the sea-air DMS flux and transfer velocity using eddy correlation, *Geophys. Res. Lett.*, *31*, L23113, doi:10.1029/2004GL021567.
Kaimal, J. C., J. C. Wyngaard, Y. Izumi, and O. R. Cote (1972), Spectral characteristics of surface-layer turbulence, *Q. J. R. Meteorol. Soc.*, *98*, 563.
Kettle, A. J., and M. O. Andreae (2000), Flux of dimethylsulfide from the oceans: A comparison of updated data sets and flux models, *J. Geophys. Res.*, *105*, 26,793.
Kondo, J. (1975), Air-sea bulk transfer coefficients in diabatic conditions, *J. Boundary Layer Meteorol.*, *9*, 91.
Lenschow, D. H. (1995), Micrometeorological techniques for measuring biosphere-atmosphere trace gas exchange, in *Biogenic Trace Gases: Measuring Emission from Soil and Water*, edited by P. A. Matson and R. C. Harris, pp. 126, Blackwell Sci., Malden, Mass.
Lenschow, D. H., and M. R. Raupach (1991), The attenuation of fluctuations in scalar concentrations through sampling tubes, *J. Geophys. Res.*, *96*, 15,259.
Liss, P. S., and L. Merlivat (1986), Air-sea gas exchange rates: Introduction and synthesis, in *The Role of Air-Sea Exchange in Geochemical Cycling*, edited by P. Buat-Menard, pp. 113, Springer, New York.
Marandino, C. A., W. J. De Bruyn, S. D. Miller, M. J. Prather, and E. S. Saltzman (2005), Oceanic uptake and the global atmospheric acetone budget, *Geophys. Res. Lett.*, *32*, L15806, doi:10.1029/2005GL023285.
Massman, W. J. (1991), The attenuation of concentration fluctuations in turbulent flow through a tube, *J. Geophys. Res.*, *96*, 15,269.
Matrai, P. A., D. J. Cooper, and E. S. Saltzman (1996), Frontal enhancement of dimethylsulfide concentrations across a Gulf Stream meander, *J. Mar. Syst.*, *7*, 1.
McGillis, W. R., J. W. H. Dacey, N. M. Frew, E. J. Bock, and R. K. Nelson (2000), Water-air flux of dimethylsulfide, *J. Geophys. Res.*, *105*, 1187.
McGillis, W. R., J. B. Edson, J. E. Hare, and C. W. Fairall (2001), Direct covariance air-sea CO_2 fluxes, *J. Geophys. Res.*, *106*, 16,729.

McMillen, R. T. (1988), An eddy correlation technique with extended applicability to non-simple terrain, *Boundary Layer Meteorol.*, *43*, 231.

Mitchell, G. M. (2001), Determination of vertical fluxes of sulfur dioxide and dimethylsulfide in the remote marine atmosphere by eddy correlation and an airborne isotopic dilution atmospheric pressure ionization mass spectrometer, Ph.D. thesis, 234 pp., Drexel Univ., Philadelphia, Pa.

Nightingale, P. D., G. Malin, C. S. Law, A. J. Watson, P. S. Liss, M. I. Liddicoat, J. Boutin, and R. C. Upstill-Goddard (2000), In situ evaluation of air-sea gas exchange parameterizations using novel conservative and volatile tracers, *Global Biogeochem. Cycles*, *14*, 373.

Pedreros, R., G. Dardier, H. Dupuis, H. C. Graber, W. M. Drennan, A. Weill, C. Guérin, and P. Nacass (2003), Momentum and heat fluxes via the eddy correlation method on the R/V *L'Atalante* and an ASIS buoy, *J. Geophys. Res.*, *108*(C11), 3339, doi:10.1029/2002JC001449.

Quinn, P. K., T. S. Bates, J. E. Johnson, D. S. Covert, and R. J. Charlson (1990), Interactions between the sulfur and reduced nitrogen cycles over the central Pacific Ocean, *J. Geophys. Res.*, *95*, 16,405.

Sakai, R. K., D. R. Fitzjarrald, and K. E. Moore (2001), Importance of low-frequency contributions to eddy fluxes observed over rough surfaces, *J. Appl. Meteorol.*, *40*, 2178.

Saltzman, E. S., D. B. King, K. Holmen, and C. Leck (1993), Experimental determination of the diffusion coefficient of dimethylsulfide in water, *J. Geophys. Res.*, *98*, 16,481.

Sunner, J., G. Nicol, and P. Kebarle (1988a), Factors determining relative sensitivity of analytes in positive mode atmospheric pressure ionization mass spectrometry, *Anal. Chem.*, *60*, 1300.

Sunner, J., M. G. Ikonomou, and P. Kebarle (1988b), Sensitivity enhancements obtained at high temperatures in atmospheric pressure ionization mass spectrometry, *Anal. Chem.*, *60*, 1308.

Upstill-Goddard, R. C., T. Frost, G. R. Henry, M. Franklin, J. C. Murrell, and N. J. P. Owens (2003), Bacterioneuston control of air-water methane exchange determined with a laboratory gas exchange tank, *Global Biogeochem. Cycles*, *17*(4), 1108, doi:10.1029/2003GB002043.

Wanninkhof, R. (1992), Relationship between wind speed and gas exchange over the ocean, *J. Geophys. Res.*, *97*, 7373.

Wanninkhof, R., J. R. Ledwell, and W. S. Broecker (1985), Gas exchange-wind speed relationship measured with sulfur hexafluoride on a lake, *Science*, *227*, 1224.

Watanabe, S., H. Yamamoto, and S. Tsunogai (1995), Dimethyl sulfide widely varying in surface water of the eastern North Pacific, *Mar. Chem.*, *51*, 253.

Watson, A. J., R. C. Upstill-Goddard, and P. S. Liss (1991), Air sea gas exchange in rough and stormy seas measured by a dual tracer technique, *Nature*, *349*, 145.

Webb, E. K., G. I. Pearman, and R. Leuning (1980), Correction of flux measurements for density effects due to heat and water vapour transfer, *Q. J. R. Meteorol. Soc.*, *106*, 85.

Yvon, S. A., and E. S. Saltzman (1996), Atmospheric sulfur cycling in the tropical Pacific marine boundary layer (12°S, 135°W): A comparison of field data and model results 2. Sulfur dioxide, *J. Geophys. Res.*, *101*(D3), 6911.

Zemmelink, H. J., W. W. C. Gieskes, W. Klaassen, W. J. Beukema, H. W. de Groot, H. J. W. de Baar, E. J. Hintsa, W. R. McGillis, and J. W. H. Dacey (2004), Relaxed eddy accumulation measurements of the sea-to-air transfer of dimethylsulfide over the northeastern Pacific, *J. Geophys. Res.*, *109*, C01025, doi:10.1029/2002JC001616.

Zhou, X., and K. Mopper (1997), Photochemical production of low-molecular-weight carbonyl compounds in seawater and surface microlayer and their air-sea exchange, *Mar. Chem.*, *56*, 201.

_____

W. J. De Bruyn, Department of Physical Sciences, Chapman University, Orange, CA 92866, USA.

C. A. Marandino and E. S. Saltzman, Department of Earth System Science, University of California, Irvine, CA 92697, USA. (cmarandi@uci.edu)

S. D. Miller, Atmospheric Sciences Research Center, Albany, NY 12203, USA.